Observations of energetic electrons up to 200 keV associated with a secondary island near the center of an ion diffusion region: A Cluster case study

Rongsheng Wang,[1,2] Quanming Lu,[1] Xing Li,[2] Can Huang,[1] and Shui Wang[1]

Received 17 March 2010; revised 13 June 2010; accepted 23 July 2010; published 5 November 2010.

[1] An antiparallel reconnection event is recognized in the magnetotail, and a secondary island with a strong core magnetic field is identified near the center of the ion diffusion region. In the island, the electron density peaks in the outer region while the dip is in the core region with a strong core magnetic field. A strong electron beam parallel to the magnetic field, as well as an obvious current antiparallel to the magnetic field with density up to ~40 nA/m^2, is observed in the outer region of the island. This suggests that the strong core magnetic field inside the island is generated by the electron beam and then the antiparallel current in the outer region of the island. The electron density dip in the core region is formed due to the existing strong core field, which expels electrons out of the core region. The electron flat-top distributions are detected in the ion diffusion region except the core region of the island, and the shoulder energy range of the flat-top distributions is from 100 eV to 4 keV. An enhancement of the energetic electron flux up to 200 keV is found in the ion diffusion region, and a further increase of energetic electron fluxes is observed inside the island. Waves at the lower hybrid frequency are intensified in the ion diffusion region, while the intensification is strong in the outer region of the island and becomes very weak in the core region.

Citation: Wang, R., Q. Lu, X. Li, C. Huang, and S. Wang (2010), Observations of energetic electrons up to 200 keV associated with a secondary island near the center of an ion diffusion region: A Cluster case study, *J. Geophys. Res.*, *115*, A11201, doi:10.1029/2010JA015473.

1. Introduction

[2] Magnetic reconnection is believed to be the main driving mechanism for many explosive phenomena in space physics and laboratory plasma physics [*Giovanelli*, 1946; *Nishida*, 1978; *Wesson*, 1997]. In the course of magnetic reconnection, stored magnetic energy is converted into plasma kinetic and thermal energy, and magnetic topology also changes [*Vasyliunas*, 1975; *Priest and Forbes*, 2000]. In solar flares, observations have confirmed that up to 50% of the released energy is carried by energetic electrons [*Lin et al.*, 1976, 2003; *Holman et al.*, 2003]. Energetic electrons have also been detected around the reconnection site in the magnetotail [*Øieroset et al.*, 2002; *Taylor et al.*, 2006; *Imada et al.*, 2007; *Åsnes et al.*, 2008; *Wang et al.*, 2008b, 2010a]. But how the electrons are accelerated in the process of magnetic reconnection is still an issue.

[3] Over the last several decades, several acceleration mechanisms have been proposed to interpret the production of the energetic electrons in magnetic reconnection [*Speiser*, 1965; *Deeg et al.*, 1991; *Litvinenko*, 1996; *Hoshino et al.*, 2001a, 2005; *Ricci et al.*, 2003; *Drake et al.*, 2005, 2006a; *Fu et al.*, 2006; *Pritchett*, 2006a, 2006b]. One is that electrons drifting into the electron diffusion region are accelerated by the reconnection electric field. Simulations have demonstrated that electrons can be accelerated to high energy by the reconnection electric field [*Speiser*, 1965; *Deeg et al.*, 1991; *Litvinenko*, 1996; *Hoshino et al.*, 2001a; *Ricci et al.*, 2003; *Fu et al.*, 2006]. However, it will cause an asymmetric distribution of energetic electrons along the direction of the electric field. This asymmetric distribution of energetic electrons has not been observed by spacecrafts. Moreover, electrons can only be accelerated inside the relatively small electron diffusion region, which cannot explain the extensive distribution of the energetic electrons in solar flares and the magnetotail [*Chen et al.*, 2009, *Huang et al.*, 2010]. *Hoshino et al.* [2001a] further proposed a two-step acceleration mechanism. They concluded that electrons are firstly accelerated inside the electron diffusion region by the reconnection electric field and are then accelerated in the pileup region due to the significant curvature and gradient drifts along the electric field. As demonstrated by the Cluster measurement, energetic electrons indeed peak near the pileup region in magnetic reconnection [*Imada et al.*, 2007; *Wang et al.*, 2008a]. Furthermore, multiple interactions of

[1]CAS Key Laboratory of Basic Plasma Physics, School of Earth and Space Sciences, University of Science and Technology of China, Hefei, Anhui, China.
[2]Institute of Mathematics and Physics, Aberystwyth University, Aberystwyth, UK.

0148-0227/10/2010JA015473

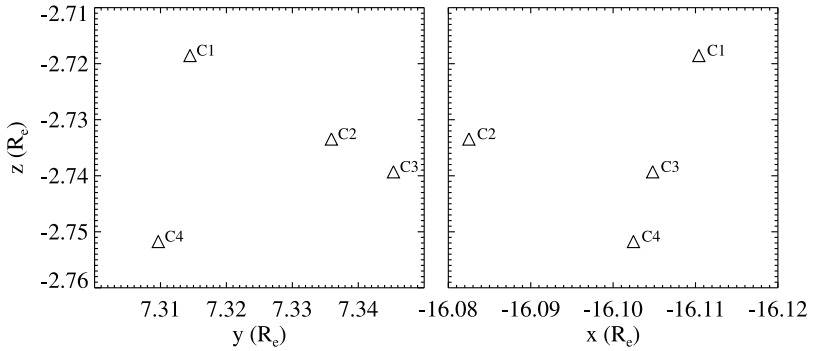

Figure 1. Positions of the Cluster spacecraft at 0619 UT on 4 October 2003 are shown in GSM coordinates. The left and right boxes show the projection of the Cluster spacecraft in the GSM *y*-*z* and *x*-*z* planes, respectively.

electrons with the density cavities along the separatrices can generate energetic electrons during reconnection with a strong guide field [*Drake et al.*, 2005].

[4] More recently, *Drake et al.* [2006a] suggested that electrons can be accelerated by the contracting magnetic islands during magnetic reconnection due to the Fermi acceleration. As a result, the energetic electrons display a field-aligned anisotropic distribution inside the islands. The fluxes of energetic electrons along the magnetic field are much greater than that perpendicular to the magnetic field, and the parallel temperature is higher than the perpendicular temperature. The relations between magnetic islands and energetic electrons have been validated by Cluster [*Zong et al.*, 2004; *Chen et al.*, 2008, 2009; *Wang et al.*, 2010a]. The measurements indicate that the fluxes of energetic electrons peak at the electron density compression sites within the magnetic islands, and the electron distribution is isotropic within islands [*Chen et al.*, 2008 and 2009], which is inconsistent with the predication of *Drake et al* [2006a]. *Chen et al.* [2009] argued that the observed energetic electrons within islands might be accelerated by the inductive electric field in the strong gradient and curvature regions caused by the convection of magnetic fluxes toward the island center.

[5] In this paper, we present a reconnection event observed by Cluster in the magnetotail, ~16 R_e on 4 October 2003. In this event, a secondary island with a strong out-of-plane magnetic field (flux rope) is detected near the center of the diffusion region, which has been reported by *Wang et al.* [2010a] and considered to be the results of secondary island instability. At that time, the spacecraft separation was only about 300 km (~0.4c/ω_{pi}), which provides an excellent opportunity to reveal the details of small scale structures and the microphysics down to the ion inertial scale or even smaller. The purpose of this paper is to explore the distribution of electron density and current density, electron pitch angle distribution, energetic electrons and associated waves around the secondary island inside the diffusion region.

2. Data

[6] Data from several instruments are used. The magnetic field data are taken from the Fluxgate Magnetometer (FGM) [*Balogh et al.*, 2001]. Ion plasma data with the spin resolution are obtained from the ion Composition and Distribution Function analyzer (CODIF) instrument, which is part of the Cluster Ion Spectrometry (CIS) experiment [*Rème et al.*, 2001]. The data of energetic electron fluxes at energies from 37 to 400 keV with the 4 s spin resolution are provided by the Research with Adaptive Particle Imaging Detectors (RAPID) [*Wilken et al.*, 2001]. The low to middle energy electron data with 4 s time resolution are from the Plasma Electron and Current Experiment (PEACE) instrument [*Johnstone*, 1997]. The PEACE instrument consists of High Energy Electron Analyser (HEEA) and Low Energy Electron Analyzer (LEEA). Both sensors are mounted on diametrically opposite sides of the spacecraft. In this paper, we will use the PITCH_SPIN data, which contain merged data from both the HEEA and LEEA sensors and are available nearly every spin, with twelve 15° (covering 0°–180° pitch angle) and 44 energy bins [*Fazakerley et al.*, 2010]. The electric and magnetic wave spectrograms are taken from the Spatio-Temporal Analysis of Field Fluctuations (STAFF) experiments with 1 s time resolution [*Cornilleau-Wehrlin et al.*, 1997]. The electric field data are taken from the Electric Field and Waves (EFW) instruments [*Gustafsson et al.*, 2001], which can only measure two components of the electric field E_x and E_y in the spin plane.

3. Observations and Analysis

[7] During 0618–0622 UT, on 4 October 2003, the Cluster tetrahedron was situated in [−16.1, 7.4, −2.6] R_E (Geocentric Solar Magnetospheric coordinates). Figure 1 shows the positions of the four satellites in the GSM coordinates used throughout this paper. From Figure 1, it can be seen that the C1 satellite was located in the northernmost and was farthest to the Earth. The largest spacecraft separation was only around 300 km (~0.4c/ω_{pi}).

[8] Figure 2 shows an overview of the measurements from Cluster during 0618–0622 UT. From top to bottom, three components and magnitude of the magnetic field with 1/5 s resolution, the *x* component of the proton bulk flow, and two components of the electric field are shown. During this interval, Cluster crossed the neutral sheet twice from the Southern Hemisphere ($B_x < 0$) to the Northern Hemisphere

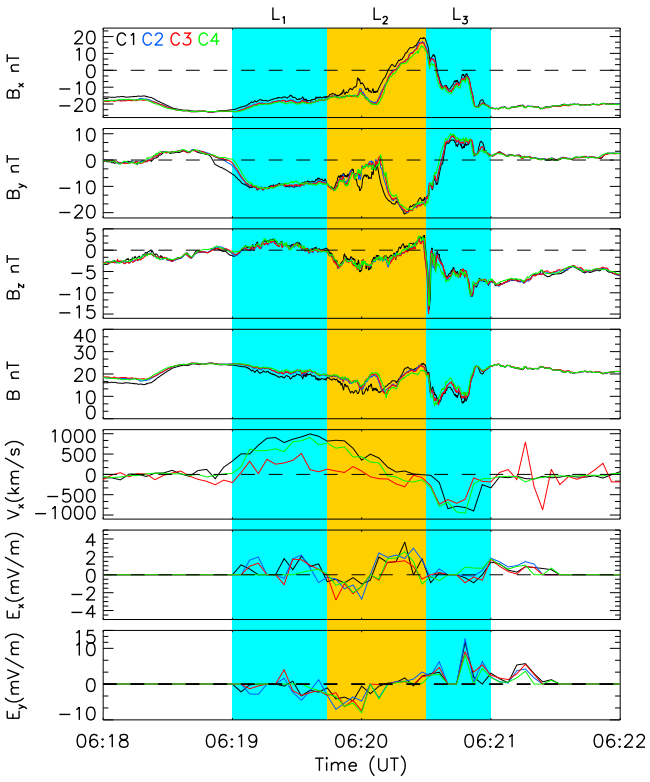

Figure 2. Overview of the electric and magnetic field and ion plasma data observed by Cluster from 0618 to 0622 UT (in GSM coordinates) with a color scheme of black, blue, red, and green for spacecrafts 1–4, respectively. From top to bottom, three components and magnitude of the magnetic field, x component proton bulk flow, and two components of the electric field E_x and E_y are shown. The L_1, L_2, and L_3 subintervals denote the times 061900–061944 UT, 061944–062030 UT and 062030–062100 UT, respectively.

($B_x > 0$), and then returned to the south ($B_x < 0$). Because the time series of magnetic field among the four satellites are well correlated, the timing analysis is applied to the magnetic field data during both crossings to calculate the normal of the neutral sheet [*Schwartz*, 1998]. The normal is n_1= [-1.715×10^{-02}, -5.019×10^{-02}, 0.999] in the GSM coordinates for the first crossing, while it is n_2 = [0.199, 0.222, −0.954] for the second crossing. Since the neutral sheet is nearly parallel to the x-y plane, the GSM coordinates are appropriate and used in this paper.

[9] The interval is characterized by a reversal of the x component of the proton bulk flow (up to 800 km/s) from earthward to tailward. Generally, the near coincident reversals of B_z and V_x indicate that the spacecraft encounters a magnetic reconnection event from one side to the other. Thus, according to the signs of B_z, the interval when the high-speed flow was observed is divided into three subintervals: L_1 (061900–061944 UT), L_2 (061944–062030 UT), and L_3 (062030–062100 UT) (corresponding to the three color regions in Figure 2). During the strong high-speed earthward flow (corresponding to the L_1), the values of B_z were mainly positive. While for the period of the high-speed tailward flow (corresponding to the L_3), the values of B_z were negative. In the L_1 period, Cluster was located to the south of the neutral sheet ($B_x < 0$), where B_y was negative. On the other hand, in the L_3 period, Cluster passed the neutral sheet from the north to the south accompanied by the sign reversals of B_y from negative in the Northern Hemisphere to positive in the Southern Hemisphere. On the basis of these measurements, the behaviors of B_y are consistent with the expected Hall magnetic field. The near coincident reversals of V_x and B_z and the organized Hall magnetic field provide a clear evidence that Cluster crossed an ion diffusion region of a collisionless magnetic reconnection event from earthward to tailward [*Wang et al.*, 2010a]. These measurements are also in accordance with previous observations [*Øieroset et al.*, 2001, 2002; *Mozer et al.*, 2002; *Runov et al.*, 2003; *Vaivads et al.*, 2004; *Borg et al.*, 2005; *Xiao et al.*, 2007; *Wang et al.*, 2010a, 2010b]. Also, note that at the beginning and the ending in Figure 2, when Cluster was in the lobe, B_y was close to zero. Thus, there is no obvious overall guide field during this magnetic reconnection event.

[10] During the L_2 period, B_z reversed from negative to positive. Besides, B_y and the magnitude of the magnetic field peaked at the point of B_z reversal. The measurements are coincided with the signature of a flux rope moving earthward. More details can be found in the paper by *Wang et al.* [2010a]. On the basis of these measurements, the approximate path of Cluster through the diffusion region is reconstructed as shown in Figure 3. The C1 satellite located at the farthest to Earth in the magnetotail detected the reversal of B_z earlier than other three satellites, which further demonstrates that the whole structure observed was moving earthward.

[11] To analyze the secondary island (flux rope) in more details, the magnetic field with time resolution 1/22 s, the electron density derived from the spacecraft potential [*Pedersen et al.*, 2008], three components of the current density calculated by the curlometer technology [*Robert et al.*, 1998], the current density parallel to the magnetic field $j_{par} = \mathbf{J} \cdot \mathbf{B}/|\mathbf{B}|$, $\nabla \cdot \mathbf{B}/|\nabla \times \mathbf{B}$, and the fluxes of energetic electrons between 061900 and 062100 UT are shown in Figure 4. The top color bars denote the three subintervals L_1, L_2, and L_3, as shown in Figure 2. The vertical dotted and dashed lines represent the reversal times of B_x and B_z within the island, respectively. In the subinterval L_2 when the island was encountered, Cluster crossed the island from the third quadrant ($B_z < 0$ and $B_x < 0$) to the first quadrant ($B_z > 0$ and $B_x > 0$), and it means that Cluster passed through the core region of the island. The interval L_2 is color coded with two different colors, orange (062012–062028 UT) and green, in terms of the signs of B_x and B_z. The orange region where B_x and B_z change their signs almost simultaneously is called the core region of the island, while the green region is called the outer region of the island in the following. In Figure 4, the electron density was gradually enhanced as Cluster approached the center of the plasma sheet from the south and was then depleted while Cluster retreated from the center of the plasma sheet to the south. The mean value of the electron density in the whole interval is about 0.2 cm^{-3}. Inside the secondary island, the electron density increased steadily as Cluster moved toward the core region but dropped sharply once the spacecraft

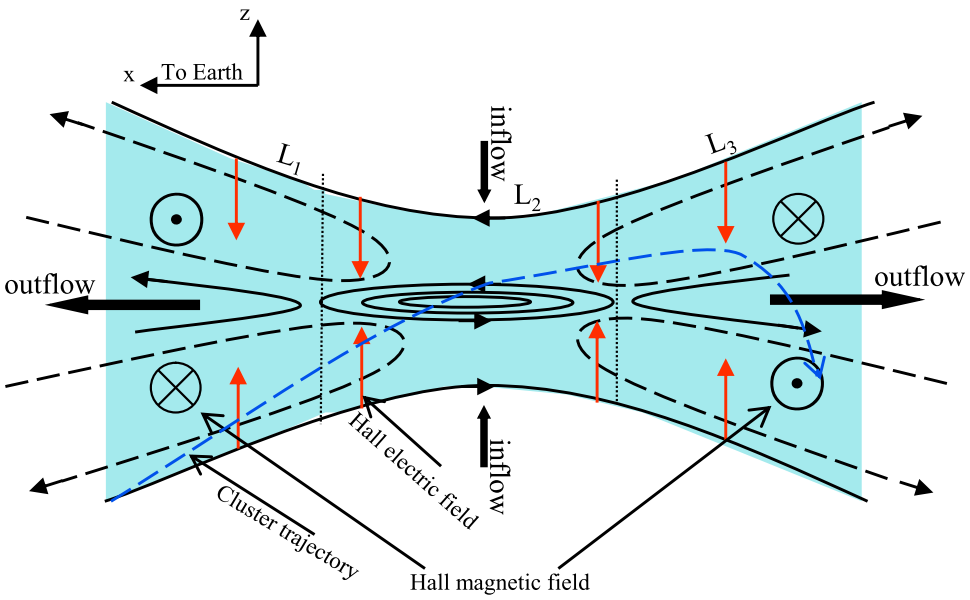

Figure 3. Schematic of the magnetic reconnection ion diffusion region and the spacecraft trajectory are shown.

entered into the core region. The maximum of the electron density in the outer region is ~0.6 cm^{-3}, while in the core region where the significant core magnetic field B_y appears the electron density holds ~0.2 cm^{-3}. Although the electron density dips in the core region, it still maintains at the average level. The C1 satellite stayed in the northernmost and farthest to the Earth relative to other satellites, thus observed the electron density dip earlier than other three satellites. This type of distribution of electron density within the island is much different from the previous measurements [*Slavin et al.*, 2003; *Zong et al.*, 2004; *Henderson et al.*, 2006; *Eastwood et al.*, 2007; *Chen et al.*, 2008, 2009; *Wang et al.*, 2008a], where the density peaks at the reversal point of B_z, and will be discussed in section 4 in more details.

[12] Both the x and y components of the electric current density increase noticeably within the island. The j_y component keeps a large positive value and the maximum value is close to ~30 nA/m^2. The j_x component, however, is augmented just in the outer region of the island and even approaches to zero in the core region. Moreover, the j_x component is positive when Cluster stays in the southern part of the outer region ($B_x < 0$), and it becomes negative when Cluster enters into the northern part of the outer region ($B_x > 0$), which suggests that the x component of the electric current density mainly directs antiparallel to the magnetic field in the outer region of the island. The electric current density parallel to the magnetic field $j_{par} = \mathbf{J} \cdot \mathbf{B}/|\mathbf{B}|$ is also shown in Figure 4. The j_{par} component is primarily negative and has a significant value in the outer region. So the electric current density is antiparallel to the magnetic field in the outer region of the island. The fact that the profile of j_{par} is similar to the j_x component indicates that the j_{par} component comes mainly from the j_x component in the outer region. In the core region with a strong core magnetic field B_y, j_{par} still has relatively high values, around 20 nA/m^2, which can be attributed to the j_y component. The ratio of $\nabla \cdot \mathbf{B}/|\nabla \times \mathbf{B}|$ has been regarded as the relative error of $\nabla J/|\mathbf{J}|$ [*Dunlop et al.*, 1990; *Chanteur*, 1998; *Xiao et al.*, 2004]. It can be found that the ratio is primarily below 0.4 inside the island. So the relative errors are low inside the island.

[13] The last four frames of Figure 4 show the fluxes of energetic electrons in the energy range 37–400 keV from the four satellites: C1, C2, C3, and C4. The different color curves express different energy channels, and the numbers on the right-hand side of Figure 4 correspond to the energy thresholds for the energy channels. The gradual enhancement (decrease) of the fluxes of energetic electrons up to 200 keV as the spacecraft approached (left) the ion diffusion region indicates that energetic electrons were being continually produced inside the diffusion region. The fact that the energetic electron fluxes inside the island are more enhanced demonstrates that electrons were further accelerated within the island [*Wang et al.*, 2010a]. Unfortunately, there were no pitch angle distribution data of the energetic electrons during the interval. However, the relatively low-energy electron pitch angle data from the PEACE instrument is available, which might provide some clues to understand the acceleration mechanism of electrons.

[14] Figure 5 shows the electron pitch angle distribution of the phase space density (PSD) from the C4 satellite at energies from 440 eV to 9.78 keV, and the similar distribution can also be found by C1 and C2 satellites (not shown here, there is no pitch angle data from the C3 satellite in this interval). Each frame shows the electron pitch angle distribution for certain energy. In the L_1 period, there is a field-aligned beam parallel to the magnetic field in the distribution from 682 eV to 2.59 keV. During this period, Cluster was located in the separatrix region. The electron beam parallel to the magnetic field is consistent with the Hall electric current directed to the X line. The field-aligned bidirectional distribution emerges in the L_2 period, where the PSD intensifies at 0^o and 180^o and are larger than that at ~90^o from 440 eV

to 2.59 keV. The field-aligned bidirectional distribution indicates that more electrons are accelerated along the magnetic field. During the L_3 interval, the field-aligned bidirectional distribution becomes less obvious.

[15] Figure 6 shows the evolution of electron spectra as C4 satellite crossed the ion diffusion region from the earthward side to the tailward side. We select three typical times for each subinterval. Figures 6a–6c, 6d–6f, and 6g–6i correspond to the subintervals L_1, L_2, and L_3, respectively. At the beginning of the L_1 interval (at 061859 UT, Figure 6a), the spacecraft staying on the boundary of the diffusion region observed the nearly isotropic distribution. The PSD decreased abruptly around 80 eV. This type of distribution was observed again when the spacecraft arrived at the opposite boundary of the diffusion region at 062059 UT (Figure 6i). After the spacecraft entered into the diffusion region, the distribution had the flat-top feature: the PSD was almost constant between 100 eV and 2 keV but sharply decreased at the both ends of the energy range. The flat-top distribution could be persistently measured until the spacecraft got into the outer region of the island from 061903 to 062007 UT, as shown in Figures 6b–6d. The flat-top distribution is anisotropic. The fluxes parallel and antiparallel to the magnetic field are larger than that perpendicular to the magnetic field with energies from 400 eV and 2 keV, regardless of the spacecraft locating in the L_1 interval or the outer region of the island. After the spacecraft entered into the core region of the island, the distribution displayed an exponential feature (Figures 6e and 6f) instead of the flat-top feature. The steep decrease of the PSD at the ends of the energy shoulder of the flat-top distribution vanished. In lower energy from 400 eV to 1 keV, the PSD along parallel direction was much larger than at other two directions. The PSD at parallel and antiparallel directions were larger than that at the perpendicular direction between 1 and 2 keV. In the L_3 interval, the flat-top distribution was observed again. However, the energy range of the shoulder of the flat-top distribution extended to higher energy from 100 eV to 4 keV. The measurements indicate that the flat-top distribution is observed in the ion diffusion region except at the core region of the island where the exponential distribution was observed, and the energy range of the shoulder of the flat-top distribution detected in the tailward side extended to higher energy than that observed in the earthward side.

[16] Figure 7 shows the magnetic field and the wave spectrogram of the electric and magnetic field from C4 satellite during the crossing. Figure 7 (top) denotes three components and the magnitude of the magnetic field. Figure 7 (middle) and Figure 7 (bottom) are the wave spectrogram of the magnetic and electric field, respectively. The solid lines indicate the lower hybrid frequency. Strong wave activity in the lower hybrid frequency was observed in the L_1 period when the spacecraft was located around the separatrax region and the L_3 period when the spacecraft was around the neutral sheet. Even stronger waves in the lower hybrid frequency were

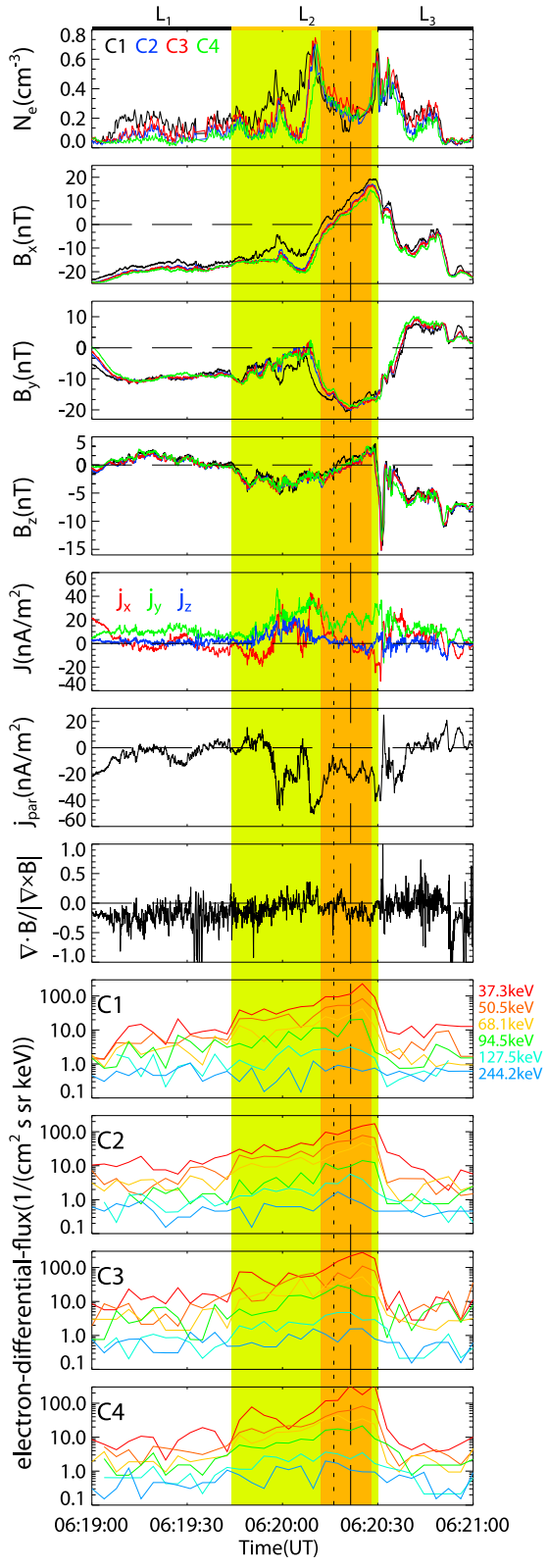

Figure 4. Cluster measurements during the interval 0619–0621 UT on 4 October 2003. The top frame shows the electron densities, and the next three frames denote three components of the magnetic field (1/22 s resolution) with the same color scheme as shown in Figure 2. The fifth and sixth frames is the three components of the current density and the parallel component of the current density, $j_{par} = \mathbf{J} \cdot \mathbf{B}/|\mathbf{B}|$. The seventh frame is the ration of $\nabla \cdot \mathbf{B}/|\nabla \times \mathbf{B}|$, regarded as the relative errors of $\Delta J/|J|$. The last four frames show the energetic electron fluxes from the four satellites, and the different colors denote the different energy thresholds.

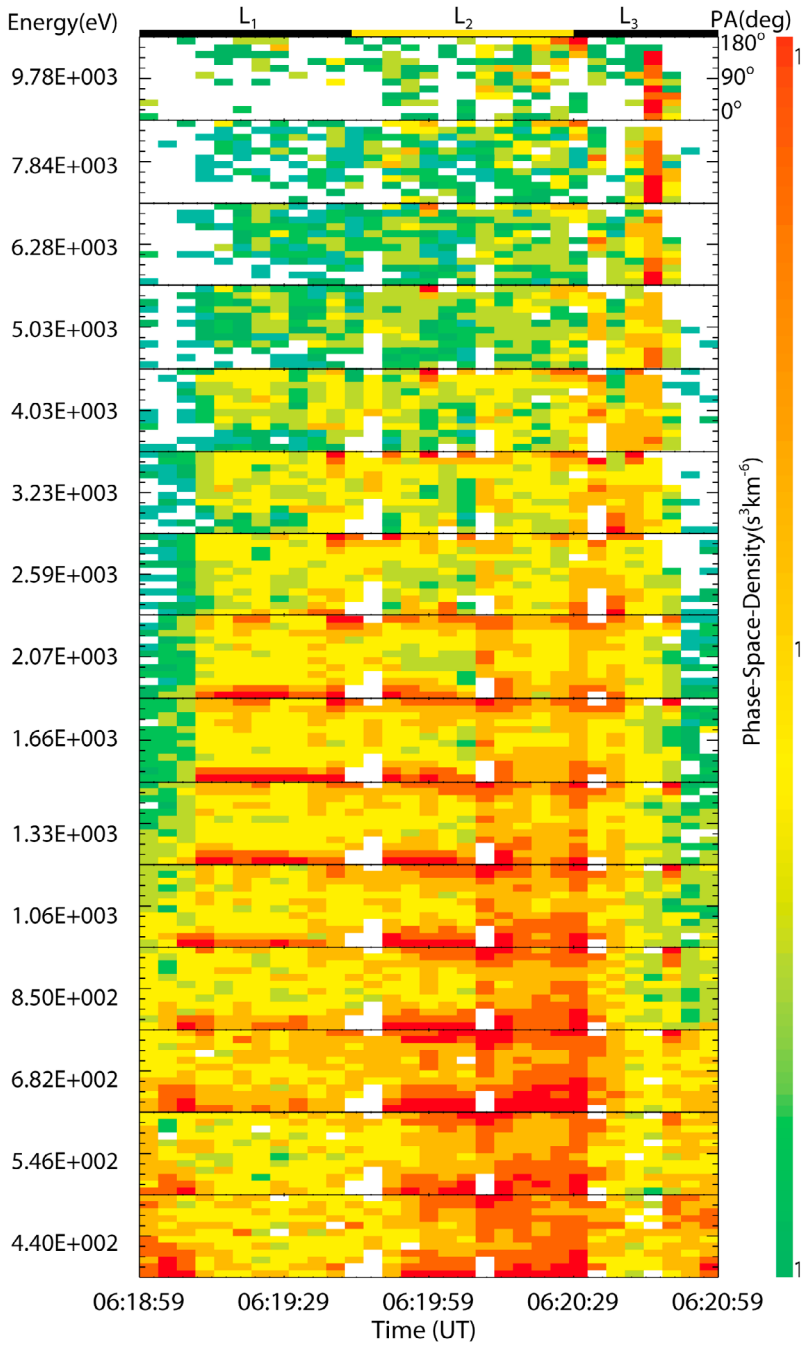

Figure 5. Electron pitch angle distributions measured by the C4 satellite from 440 eV to 7.98 keV during the interval 061859–062059 UT. The L_1, L_2, and L_3 periods correspond to the three subintervals shown in Figures 2 and 4.

detected in the outer region of the island. However, the wave activity became very weak in the core region of the island.

4. Discussion

[17] The representative observational characteristics of the island (flux rope) are bipolar B_z and strong core field B_y, which are often observed in the magnetotail accompanied with an electron density peak at the reversal point of B_z [*Slavin et al.*, 2003; *Xiao et al.*, 2004; *Zong et al.*, 2004, 2007; *Cao et al.*, 2006; *Nakamura et al.*, 2006; *Eastwood et al.*, 2007; *Chen et al.*, 2008, 2009; *Retinò et al.*, 2008; *Wang et al.*, 2008a, 2010a]. In the previous measurements, however, the B_x component often had a considerable value at the time when the value of B_z is reversed [*Slavin et al.*, 2003; *Zong et al.*, 2004; *Henderson et al.*, 2006; *Eastwood et al.*, 2007; *Chen et al.*, 2008, 2009; *Wang et al.*, 2008a], which means that the spacecraft did not cross the core region of the island. In our event, almost simultaneous reversals of B_x and B_z suggest that the spacecraft crossed the core region

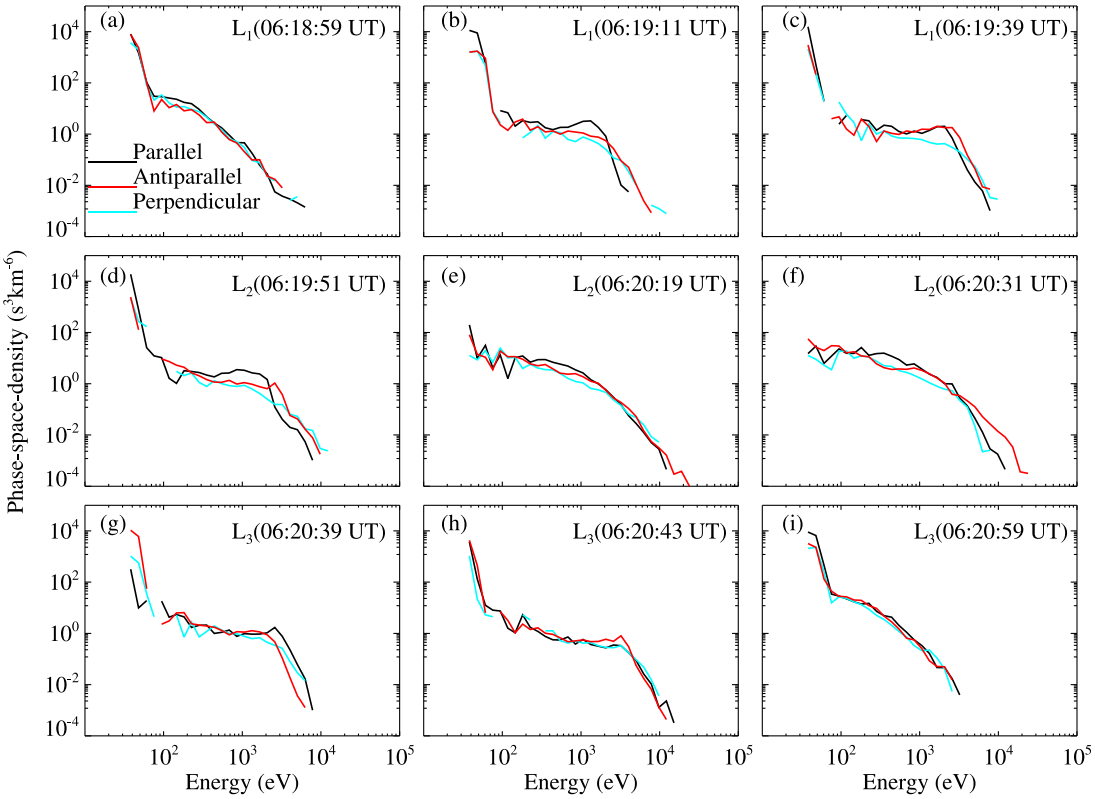

Figure 6. Electron spectra observed in the three subintervals. Shown are the samples in the (a–c) L_1, (d–f) L_2, and (g–i) L_3 periods.

of the island, which provides an opportunity to study the physics in the core region. A characteristic feature in our event is that the electron density dip arises in the core region, which was not seen in the previous observations. The reason for this difference between the previous measurements and ours may be attributed to the different trajectory of the spacecraft relative to the island.

[18] On the basis of the measurements, we conclude that the electron density peaks in the outer region and dips in the core region of the island. An illustration is shown in Figure 8. The light gray color inside the island denotes the region with smaller density, and the darker gray represents the region with higher electron density. Lines 1 and 2 represent the two trajectories of spacecraft. The electron density curves in Figure 8 indicate the evolution of the density as the spacecraft crosses the island from trajectories 1 and 2, respectively. Orbit 2 represents the trajectory of our event, while Orbit 1 denotes the trajectory in previous observations. If the

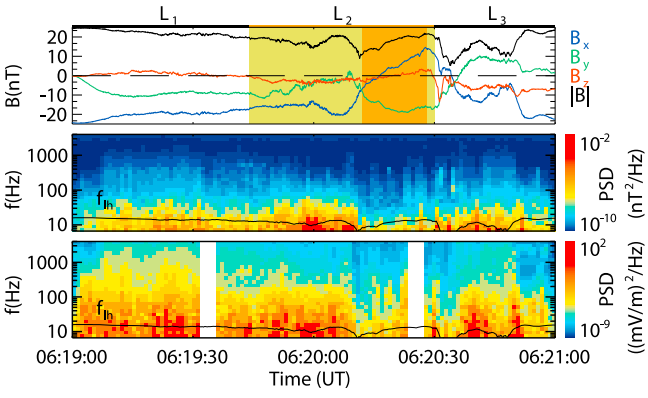

Figure 7. (top) The magnetic field from the C4 satellite. The wave spectrogram of (middle) the magnetic field and (bottom) the electric field with 1 s time resolution. The solid line in Figure 7 (middle) and 7 (bottom) is the lower hybrid frequency.

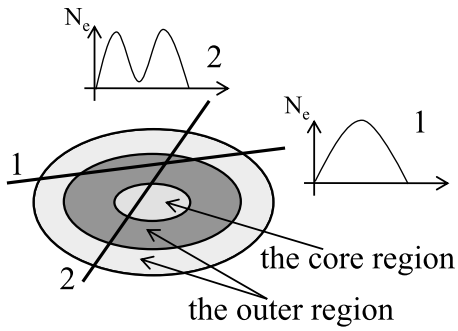

Figure 8. The illustration of the electron density distribution inside the island. The light gray color denotes the region with smaller electron density, and the darker gray area represents the higher density area. Lines 1 and 2 express two trajectories of the spacecraft. The electron density curves indicate the evolution of the density, as the spacecraft crosses the island from trajectories 1 and 2, respectively.

spacecraft indeed enters the core region of an island (i.e., nearly simultaneous reversals of B_z and B_x or B_x close to zero in the process of reversal of B_z), the electron density dip can be observed. On the other hand, if the spacecraft just crosses the island from the outer region as in Orbit 1, a peak of the density will be observed. The measurement reported by Retinò et al confirms our conclusions [*Retinò et al.*, 2008]. In their paper, the density dip was also found in the core region of an island, but they argued that the dip was produced by the coalescence of several islands [*Retinò et al.*, 2008]. Actually, it is understandable that the strong core magnetic field existing in the core region would expel electrons out of the core region and cause the pileup of electrons in the outer region of the island.

[19] In simulations, the formation of the core field inside the island is thought to be driven by the compression of the initial guide field [*Drake et al.*, 2006b]. However, there is no obvious overall guide field in our event. The analysis of the electric current density demonstrates that the core field is produced by the antiparallel current in the outer region of the island. Using Ampere's law, we can estimate the out-of-plane magnetic field produced by the j_x component in the outer region. The propagation velocity of the island in the z direction is 52.4 km/s on the basis of the timing method [*Wang et al.*, 2010a]. The crossing time of the core region is 16 s. The size of core region of the island in the z direction is estimated to be 838.4 km. The value of j_x is about 30 nA/m^2. Hence, the out-of-plane magnetic field produced by j_x is of the order of 30 nT, consistent with the observed core field. We conclude that the strong core field is indeed created by the parallel current in the outer region. The intense electron beam parallel to the magnetic field measured in the outer region strongly suggests that the antiparallel current comes from the electron beam.

[20] According to the analysis above, the parallel electron beam in the outer region of the island forms the electric current antiparallel to the magnetic field. This electric current produces the observed strong core field, which expels the electron out of the core region. Island with a strong core field during antiparallel reconnection has also been observed [*Eastwood et al.*, 2007], where the island is located in the Hall magnetic field region. In that case, the core field is thought to be caused by the compression of the Hall magnetic field.

[21] The flat-top distribution has been reported in other literatures [*Smets et al.*, 1998; *Asano et al.*, 2008; *Chen et al.*, 2009]. According to early observations, the flat-top distribution is mainly located near the outer boundary of the ion diffusion region in the plasma sheet outflow region, before reaching the pileup region with large normal component of the magnetic field [*Asano et al.*, 2008]. *Chen et al.* [2009] confirmed that the isotropic flat-top distribution can also be found inside the islands. In the previous observations, the typical energies of the shoulder of the flat-top distribution are 2–10 keV [*Asano et al.*, 2008; *Chen et al.*, 2009]. In our event, the flat-top distribution can be observed almost in the entire ion diffusion region except at the core region of the island. The typical energy range of the shoulder is just from 80 eV to 2 keV in the earthward side and expands to 4 keV in the tailward side. The flat-top distribution is always accompanied by the electron beam in the L_1 interval, which is in accordance with the predication by *Hoshino et al.* [2001b], who suggest that the flat-top distribution is the thermalized component of the electron beam toward the X line. In the L_3 period, when the spacecraft is located around the neutral sheet, the flat-top distribution can still be observed and the shoulder energy even expands to higher energy. Around the neutral sheet (the L_3 interval), more low-energy electrons are accelerated, so the shoulder energy of the flat-top distribution can expand to higher energy. Electrons with the lower energy (100–600 eV in the earthward, 100–800 eV in the tailward of the diffusion region) are accelerated to the higher energy (600 eV–2 keV in the earthward, 100 eV–4 keV in the tailward of the diffusion region). Consequently, the PSD at the lower energy declines whereas that at the higher energy increases, which leads to the constant PSD over the whole energy range from 100 eV to 2 keV in the earthward and from 100 eV to 4 keV in the tailward of the diffusion region. Thus, the flat-top distribution is formed. The measurements of the spectra indicate that in the ion diffusion region, except the core region of the island, electrons are accelerated and the flat-top distribution is formed, while the PSD of electrons displays the exponential feature in the core region of the island. Very recently, *Egedal et al.* [2010] proposed that a positive acceleration potential in the vicinity of the reconnection site could form the observed flat-top distributions.

[22] Recently, *Drake et al.* [2006a] proposed that the contracting islands can accelerate electrons to relativistic energy by the Femi acceleration. In their model, only electrons with large parallel velocity $v_{\|} > u_x \approx c_{Ax}$ (corresponding to the energy of 10 keV in the magnetotail, the c_{Ax} and u_x are the Alfven speed and the contracting velocity of the ends of magnetic island, respectively) can obtain high energy by interacting with multiple islands. According to the model, electrons with large parallel velocity will be accelerated along the magnetic field and the parallel temperature is higher than that in the perpendicular direction. In our event, the parallel temperature is indeed larger than the perpendicular temperature [*Wang et al.*, 2010a]. However, the powerful field-aligned bidirectional distribution inside the island merely arises in the low-energy range between 440 eV and 2.59 keV and disappears in the higher energy. Because of the absence of the pitch angle distribution for energetic electrons larger than 20 keV, we cannot confirm whether the distribution of energetic electrons larger than 20 keV is consistent with the prediction of the Femi acceleration or not. *Huang et al.* [2010] suggested that the inductive electric fields would accelerate electrons when electrons passed the strong magnetic gradient and curvature region inside the islands. In our event, the E_y can reach 10 mV/m by which an electron could gain 100 keV energy just over $14c/\omega_{pi}$ ($\sim 1.5R_E$). Hence, the inductive electric field might be very important for the production of the energetic electrons.

5. Conclusions

[23] A reconnection event with no obvious overall guide field in the near-Earth magnetotail is presented. Near the center of the ion diffusion region, an island with a strong core magnetic field is detected. Using the high time resolution electron density data, it is found that the electron density dips in the core region of the island and pileups in the outer region. The current density antiparallel to the magnetic field is considerable in the outer region of the island. At the same time, a

strong electron beam parallel to the magnetic field is also observed in the outer region. We conclude that the electron beam parallel to the magnetic field yields the strong antiparallel current. This current will produce an out-of-plane core field inside the island. Because of the strong core field, parts of electrons are expelled out of the core region and pile up in the outer region.

[24] The fluxes of energetic electrons up to 200 keV were gradually enhanced as the spacecraft crossed the diffusion region and a further enhancement can be found inside the secondary island. The flat-top distribution of electrons is observed in the ion diffusion region except at the core region of the island, where the exponential distribution is measured. The shoulder energy is between 80 eV and 2 keV in the L_1 interval and expands to higher energy (~4 keV) in the L_3 interval. The lower energy part of electrons (80–600 eV) is accelerated to the higher energy (600 eV to 2 keV). As a result, the PSD of the lower (higher) energy electrons decreases (enhances), which causes the equal level of the PSD over the whole energy range from 80 eV to 2 keV. The shoulder energy observed around the neutral sheet (corresponding to the L_3 interval) can expand to higher energy than that observed in the separatrix region (corresponding to the L_1 interval). The strong wave spectrogram of the electromagnetic field at the lower hybrid frequency is observed in the ion diffusion region (out of the island). The wave spectrogram is further enhanced in the outer region but becomes very weak in the core region of the island. The relations between energetic electrons and lower hybrid waves are beyond the scope of the paper and need further investigations.

[25] **Acknowledgments.** This work was supported by the Chinese Academy of Sciences under grant KJCX2-YW-N28 and the National Science Foundation of China (NSFC) under grants 40725013 and 40931053. All Cluster data are obtained from the ESA Cluster Active Archive. We thank the FGM, CIS, PEACE, RAPID, STAFF, and EFW instrument teams and the ESA Cluster Active Archive.

[26] Philippa Browning thanks the reviewers for their assistance in evaluating this paper.

References

Åsnes, A., M. G. G. T. Taylor, A. L. Borg, B. Lavraud, R. W. H. Friedel, C. P. Escoubet, H. Laakso, P. Daly, and A. N. Fazakerley (2008), Multispacecraft observation of electron beam in reconnection region, *J. Geophys. Res.*, *113*, A07S30, doi:10.1029/2007JA012770.

Asano, Y., et al. (2008), Electron flat-top distributions around the magnetic reconnection region, *J. Geophys. Res.*, *113*, A01207, doi:10.1029/2007JA012461.

Balogh, A., et al. (2001), The Cluster magnetic field investigation: Overview of in-flight performance and initial results, *Ann. Geophys.*, *19*, 1207–1217.

Borg, A. L., M. Øieroset, T. D. Phan, F. S. Mozer, A. Pedersen, C. Mouikis, J. P. McFadden, C. Twitty, A. Balogh, and H. Rème (2005), Cluster encounter of a magnetic reconnection diffusion region in the near-Earth magnetotail on September 19, 2003, *Geophys. Res. Lett.*, *32*, L19105, doi:10.1029/2005GL023794.

Cao, J. B., et al. (2006), Joint observations by Cluster satellites of bursty bulk flows in the magnetotail, *J. Geophys. Res.*, *111*, A04206, doi:10.1029/2005JA011322.

Chanteur, G. (1998), *Spatial Interpolation for Four Spacecraft: Theory Analysis Methods for Multi-Spacecraft Data*, *ISSI Sci. Rep. SR-001*, edited by G. Paschmann and P. W. Daly, Eur. Space Agency, Paris.

Chen, L.-J., et al. (2008), Observation of energetic electrons within magnetic islands, *Nature Phys.*, *4*, 19–23, doi:10.1038/nphys777.

Chen, L. J. et al. (2009), Multispacecraft observations of the electron current sheet, neighboring magnetic islands, and electron acceleration during magnetotail reconnection, *Phys. Plasmas*, *16*, 056501.

Cornilleau-Wehrlin, N., et al. (1997), The Cluster Spatio-Temporal Analysis of Field Fluctuations (STAFF) experiment, *Space Sci. Rev.*, *79*, 107–136.

Deeg, H. J., J. E. Borovsky, and N. Duric (1991), Particle acceleration near X-type magnetic neutral lines, *Phys. Fluids B*, *3*, 2660–2674.

Drake, J. F., M. A. Shay, W. Thongthai, and M. Swisdak (2005), Production of energetic electrons during magnetic reconnection, *Phys. Rev. Lett.*, *94*, 095001

Drake, J. F., M. Swisdak, H. Che, and M. A. Shay (2006a), Electron acceleration from contracting magnetic islands during reconnection, *Nature*, *443*(7111), 553–556.

Drake, J. F., M. Swisdak, K. M. Schoeffler, B. N. Rogers, and S. Kobayashi (2006b), Formation of secondary islands during magnetic reconnection, *Geophys. Res. Lett.*, *33*, L13105, doi:10.1029/2006GL025957.

Dunlop, M. W., A. Balogh, D. J. Southwood, R. C. Elphic, K.-H. Glassmeier, and F. M. Neubauer (1990), Configurational sensitivity of multipoint magnetic field measurements, in *Proceedings of the International Workshop on Space Plasma Physics Investigations by Cluster and Regatta*, *ESA SP-306*, pp. 23–28, Eur. Space Agency, Paris.

Eastwood, J. P., T.-D. Phan, F. S. Mozer, M. A. Shay, M. Fujimoto, A. Retino, M. Hesse, A. Balogh, E. A. Lucek, and I. Dandouras (2007), Multipoint observations of the Hall electromagnetic field and secondary island formation during magnetic reconnection, *J. Geophys. Res.*, *112*, A06235, doi:10.1029/2006JA012158.

Egedal, J., A. Lê, N. Katz, L.-J. Chen, B. Lefebvre, W. Daughton, and A. Fazakerley (2010), Cluster observations of bidirectional beams caused by electron trapping during antiparallel reconnection, *J. Geophys. Res.*, *115*, A03214, doi:10.1029/2009JA014650.

Fazakerley, A. N., et al. (2010), PEACE Data in the Cluster Active Archive, in *The Cluster Active Archive*, edited by H. Laakso, M. G. T. T. Taylor, and C. P. Escoubet, pp. 129–143, Springer, Netherlands.

Fu, X. R., Q. M. Lu, and S. Wang (2006), The process of electron acceleration during collisionless magnetic reconnection, *Phys. Plasmas*, *13*, 012309.

Giovanelli, R. G. (1946), A theory of chromospheric flares, *Nature*, *158*, 81–82.

Gustafsson, G., et al. (2001), First results of electric field and density observations by Cluster EFW based on initial months of operation, *Ann. Geophys.*, *19*, 1219–1240.

Henderson, P. D., C. J. Owen, L. V. Alexeev, J. A. Slavin, A. N. Fazakerley, E. A. Lucek, and H. Rème (2006), Cluster observations of flux rope structures in the near-tail, *Ann. Geophys.*, *24*, 651–666.

Holman, G. D., L. H. Sui, R. A. Schwartz, and A. G. Emslie (2003), Electron bremsstrahlung hard X-ray spectra, electron distributions, and energetics in the 2002 July 23 solar flare, *Astrophys J.*, *595*(2), L97–L101.

Hoshino, H., T. Mukai, T. Terasawa, and I. Shinohara (2001a), Suprathermal electron acceleration in magnetic reconnection, *J. Geophys. Res.*, *106*(A11), 25,979–25,997, doi:10.1029/2001JA90005.

Hoshino, M., K. Hiraide, and T. Mukai (2001b), Strong electron heating and non-Maxwellian behavior in magnetic reconnection, *Earth Planets Space*, *53*, 627–634.

Hoshino, M. (2005), Electron surfing acceleration in magnetic reconnection, *J. Geophys. Res.*, *110*, A10215, doi:10.1029/2005JA011229.

Huang, C., Q. M. Lu, and S. Wang (2010), The mechanisms of electron acceleration in antiparallel and guide field magnetic reconnection, *Phys. Plasmas*, *17*, 072306, doi:10.1063/1.3457930.

Imada, S., R. Nakamura, P. W. Daly, M. Hoshino, W. Baumjohann, S. Muhlbachler, A. Balogh, and H. Rème (2007), Energetic electron acceleration in the downstream reconnection outflow region, *J. Geophys. Res.*, *112*, A03202, doi:10.1029/2006JA011847.

Johnstone, A. D. (1997), PEACE: A plasma electron and current experiment, *Space Sci. Rev.*, *79*, 351–398.

Lin, R. P., and H. S. Hudson (1976), Nonthermal process in large solar flares, *Sol. Phys.*, *50*, 153–178.

Lin, R. P., et al. (2003), RHESSI observations of particle acceleration and energy release in an intense solar gamma-ray line flare, *Astrophys J.*, *595*(2), L69–L76.

Litvinenko, Y. E. (1996), Particle acceleration in reconnecting current sheets with a nonzero magnetic field, *Astrophys. J.*, *462*, 997.

Mozer, F. S., S. D. Bale, and T. D. Phan (2002), Evidence of diffusion regions at a subsolar magnetopause crossing, *Phys. Rev. Lett.*, *89*, doi:10.1103/PhysRevLett.89.015002.

Nakamura, R., W. Baumjohann, Y. Asano, A. Runov, A. Balogh, C. J. Owen, A. N. Fazakerley, M. Fujimoto, B. Klecker, and H. Réme (2006), Dynamics of thin current sheets associated with magnetotail reconnection, *J. Geophys. Res.*, *111*, A11206, doi:10.1029/2006JA011706.

Nishida, A. (1978), *Geomagnetic Diagnostics of the Magnetosphere*, Springer, New York.

Øieroset, M., et al. (2001), In situ detection of collisionless reconnection in the Earth's magnetotail, *Nature*, *412*, 414–417.

Øieroset, M., R. P. Lin, T. D. Phan, D. E. Larson, and S. D. Bale (2002), Evidence for electron acceleration up to ~300 keV in the magnetic reconnection diffusion region of Earth's magnetotail, *Phys. Rev. Lett.*, *89*, 195001.

Pedersen, A., et al. (2008), Electron density estimations derived from spacecraft potential measurements on Cluster in tenuous plasma regions, *J. Geophys. Res.*, *113*, A07S33, doi:10.1029/2007JA012636.

Priest, E., and T. Forbes (2000), *Magnetic Reconnection: MHD Theory and Applications*, Cambridge Univ. Press, Cambridge, U. K.

Pritchett, P. L. (2006a), Relativistic electron production during guide field magnetic reconnection, *J. Geophys. Res.*, *111*, A10212, doi:10.1029/2006JA011793.

Pritchett, P. L. (2006b), Relativistic electron production during driven magnetic reconnection, *Geophys. Res. Lett.*, *33*, L13104, doi:10.1029/2005GL025267.

Retinò, A., et al. (2008), Cluster observations of energetic electrons and electromagnetic fields within a reconnecting thin current sheet in the Earth's magnetotail, *J. Geophys. Res.*, *113*, A12215, doi:10.1029/2008JA013511.

Rème, H., et al. (2001), First multispacecraft ion measurements in and near the Earth's magnetosphere with the identical Cluster ion spectrometry (CIS)experiment, *Ann. Geophys.*, *19*, 1303.

Ricci, P., G. Lapenta, and J. U. Brackbill (2003), Electron acceleration and heating in collisionless magnetic reconnection, *Phys Plasmas*, *10*(9), 3554–3560.

Robert, P., M. W. Dunlop, A. Roux, and G. Chanteur (1998), Accuracy of current determination, in *Analysis Methods for Multi Spacecraft Data*, edited by G. Paschmann and P. W. Daly, p. 395, Eur. Space Agency, Bern, Switzerland.

Runov, A., et al. (2003), Current sheet structure near magnetic X-line observed by Cluster, *Geophys. Res. Lett.*, *30*(11), 1579, doi:10.1029/2002GL016730.

Smets, R., D. Delcourt, and D. Fontaine (1998), Ion and electron distribution functions in the distant magnetotail: Modeling of Geotail observations, *J. Geophys. Res.*, *103*(A9), 20,407–20,417, doi:10.1029/98JA01369.

Speiser, T. W. (1965), Particle trajectories in a model current sheet, based on the open model of the magnetosphere, with applications to auroral particles, *J. Geophys. Res.*, *70*, 1717, doi:10.1029/JZ070i007p01717.

Schwartz, S. J. (1998), Shock and discontinuity normals, Mach numbers and related parameters, in *Analysis Methods for Multi-Spacecraft Data*, edited by G. Paschmann and P. W. Daly, pp. 249–270, Int. Space Sci. Inst., Bern.

Taylor, M. G. G. T., et al. (2006), Cluster encounter with an energetic electron beam during a substorm, *J. Geophys. Res.*, *111*, A11203, doi:10.1029/2006JA011666.

Vaivads, A., et al. (2004), Structure of the magnetic reconnection diffusion region from four-spacecraft observations, *Phys. Rev. Lett.*, *93*, doi:10.1103/PhysRevLett.93.105001.

Vasyliunas, V. M. (1975), Theoretical models of magnetic field line merging, *Rev. Geophys. Space Phys.*, *13*, 303.

Wang, R. S., Z. Y. Li, and C. L. Tang (2008a), Observations of multiple X lines collisionless reconnection in the near Earth-tail, *Chinese J. Geophys.*, *51*, 1121–1126.

Wang, R. S., Q. M. Lu, J. Guo, and S. Wang (2008b), Spatial distribution of energetic electrons during magnetic reconnection, *Chinese Phys. Lett.*, *25*, 3083–3085.

Wang, R. S., Q. M. Lu, A. M. Du, and S. Wang (2010a), In situ observations of a secondary magnetic island in an ion diffusion region and associated energetic electrons, *Phys. Rev. Lett.*, *104*, doi:10.1103/PhysRevLett.104.175003.

Wang, R. S., Q. M. Lu, C. Huang, and S. Wang (2010b), Multispacecraft observation of electron pitch angle distributions in magnetotail reconnection, *J. Geophys. Res.*, *115*, A01209, doi:10.1029/2009JA014553.

Wesson, J. (1997), *Tokomaks*, Oxford Univ. Press, New York.

Wilken, B., et al. (2001), First results from the RAPID imaging energetic particle spectrometer on board Cluster, *Ann. Geophys.*, *19*, 1355–1366.

Xiao, C. J., Z. Y. Pu, Z. W. Ma, S. Y. Fu, Z. Y. Huang, and Q. G. Zong (2004), Inferring of flux rope orientation with the minimum variance analysis technique, *J. Geophys. Res.*, *109*, A11218, doi:10.1029/2004JA010594.

Xiao, C. J., et al. (2007), Cluster measurements of fast magnetic reconnection in the magnetotail, *Geophys. Res. Lett.*, *34*, L01101, doi:10.1029/2006GL028006.

Zong, Q. G., et al. (2004), Cluster observations of earthward flowing plasmoid in the tail, *Geophys. Res. Lett.*, *31*, L18803, doi:10.1029/2004GL020692.

Zong, Q. G., et al. (2007), Earthward flowing plasmoid: Structure and its related ionospheric signature, *J. Geophys. Res.*, *112*, A07203, doi:10.1029/2006JA012112.

C. Huang, Q. Lu, R. Wang, and S. Wang, CAS Key Laboratory of Basic Plasma Physics, School of Earth and Space Sciences, University of Science and Technology of China, Hefei, Anhui 230026, China.

X. Li, Institute of Mathematics and Physics, Aberystwyth University, SY23 3BZ, UK.